Diyala Journal of Engineering Sciences

Journal homepage: https://djes.info/index.php/djes

ISSN: 1999-8716 (Print); 2616-6909 (Online)

Frankincense Extract as Eco-Friendly Corrosion Inhibitor for Carbon Steel in 1M HCl Solution

Ameel Al-Mayah[1*], Zainab H. Ali [2], Muthana M. Kassim[2]

[1] Department of Biochemical Engineering, Al-Khwarizmi College of Engineering, University of Baghdad
[2] Iraqi Corrosion Center, The Cooperation of Research and Industrial Development, Ministry of Industry and Minerals

ARTICLE INFO

Article history:
Received: 31/01/2025.
Revised: 25/10/2025.
Accepted: 03/11/2025.
Available online: 10/12/2025.

Keywords:
Frankincense extract
Corrosion Inhibitor
Green Inhibitor
Carbon Steel
Electrochemical Impedance Spectroscopy

ABSTRACT

Steel corrosion in acidic environments is a critical industrial challenge, necessitating effective yet eco-friendly inhibitors. This study aims to address this problem by introducing a novel, green alternative: frankincense extract (FE). The distinctive contribution of this work lies in the comprehensive investigation of FE natural, sustainable, and economically viable resin as an effective corrosion inhibitor for carbon steel in 1 M HCl. The research employs an integrated methodology, including electrochemical techniques (potentiodynamic polarization (PDP) and electrochemical impedance spectroscopy (EIS)), adsorption isotherm modeling, surface analysis (FT-IR and FESEM/EDX), and density functional theory (DFT) calculations. Key results demonstrated that FE exhibited excellent inhibition performance, achieving a remarkable efficiency of 87.2% at a concentration of 16 g/L and 303 K. PDP analysis confirmed FE acts as a mixed-type inhibitor. EIS results corroborated this performance, showing 75.89% inhibition efficiency. Adsorption behavior adhered to the Langmuir isotherm, and thermodynamic parameters revealed a spontaneous and exothermic process indicative of mixed physisorption and chemisorption mechanisms. Kinetic studies further supported this by showing an increased activation energy barrier for corrosion in the presence of the inhibitor. Surface analysis confirmed the formation of a protective adsorbed film on the steel. Quantum chemical computations provided molecular-level insights, correlating the electronic structure of key FE constituents with their adsorption strength. The study establishes FE as a cost-effective, sustainable, and highly efficient green corrosion inhibitor, offering a viable solution for protecting carbon steel infrastructure in aggressive acidic media.

1. INTRODUCTION

The steel alloys find extensive application in different industrial processes due to their superior mechanical properties. Nevertheless, when subjected to acidic aqueous conditions during their operations which include descaling, pickling and acid cleaning, they greatly accelerate the corrosion process resulting in degradation of the material [1-5]. In the industrial pickling, hydrochloric acid is especially common place as it is cost effective, reacts quickly, and yields high-quality surfaces at low temperatures, and forms soluble salts that are easy to handle as wastes [6]. Even though concentrations of between 2-5% are typical [7], HCl violently reacts with the base metal, causing massive material loss and surface damage as well as extraction of unwanted deposits [8]. Different protection methods have been applied or implemented at different levels and with success such as protective coating, cathodic protection, modifying the environment, and using inhibitors [9]. Organic and inorganic corrosion inhibitors constitute one of such among others [10]. Organic types of inhibitors usually

* Corresponding author.
E-mail address: drameel@kecbu.uobaghdad.edu.iq
DOI: 10.24237/djes.2025.18406

contain heteroatoms (i.e. nitrogen, oxygen, sulfur, phosphorus) that allow them to adsorb onto metal surfaces, whereas inorganic types of inhibitors generally promote passivation layers [11,12]. Nonetheless, most synthetic inhibitors are either environmentally unsafe, or they are complicated to prepare, which highlights the importance of effective and sustainable alternatives [13,14]. Recent research has made a tremendous contribution towards plant-based corrosion inhibitors, as the possible efficient and environmentally safe substitutes to synthetic materials. These natural extracts are phytochemical-rich natural extracts obtained by different botanical sources which mitigate corrosion by adsorption and formation of protective layers on metal surfaces [15]. Fruit and vegetable extracts are especially useful and some of them have inhibition efficiencies up to 98.8% in aggressive media [16]. Examples of this include the fact that the methanolic extract of Citrullus colocynthis fruit has been proven to offer carbon steel 93.6% protection in 1 M HCl which is due to amino acids present in it such as citrulline [17]. A study by Radouane et al. [18], on the effectiveness of Bidens aurea aiton extract as a potential green corrosion inhibitor of carbon steel in a solution of 0.5 M HCl, found that 94% effectiveness was achieved. Hala et al. [19], determine the inhibition ability of the Potentilla erecta (Tormentil) extract against the 360 carbon steel in 1M of HCl and the inhibition ability of the extract at the highest concentration of 300ppm was found to be 92.7% at 55°C. Qahtan et al. [20], examined the efficacy of safflower plant (SP) extract in carbon steel in HCl solutions. They discovered that the SP extract is a good mixed-type inhibitor, and its efficiency was 89.6% at 2.5 g/l. Khang et al. [21], investigated the extract of the Syzygium polyanthum (Wight) Walp. leaf on carbon steel in 1 M HCl solution. They discovered that extract greatly decreased corrosion efficiency of 94.65% at 2000 ppm extract. The effectiveness of certain compounds, including Curcumin derivatives of Curcuma longa, as mixed-type inhibitors, which act mainly via physical adsorption mechanism has been proven [22]. The high potency of extracts of plants like Andrographis paniculata, Moringa oleifera and Bacopa monnieri further have been supported by comprehensive reviews that have attained up to 98 percent inhibition efficiencies of carbon steel in hydrochloric acid solutions [23]. Typically, the plant extracts are viewed as rich sources of naturally occurring chemical compounds synthesized by simple and inexpensive methods and some of them show inhibition efficiencies of over 90% in acidic conditions [24]. Even considering these developments, the aromatic natural exudate frankincense resin (Family: Burseraceae) that contains boswellic acids, terpenoids, flavonoids, and other bioactive compounds with anticorrosiveness potential, has remained underutilized [25-29]. This paper fills this research gap by evaluating the systematically frankincense extract (FE) as a green corrosion inhibitor to carbon steel in 1 M HCl at temperature between 303 to 333 K. The inhibitor was made following an easy and eco-friendly process. It used a multidisciplinary approach and included electrochemical (EIS, potentiodynamic polarization) and adsorption isotherm modeling, FT-IR spectroscopy, and surface characterization through FESEM/EDX. The DFT results were used to understand the interfaces and the adsorption mechanisms on a molecular level as well as the stability of the interface. The study will also seek to add to the creation of effective and environmental corrosion inhibition approaches to be used in industry by combining experimental and theoretical studies.

2. METHODOLOGY

2.1 Materials and Equipment

The FE was obtained by soaking 100 g of fresh Frankincense in 1000 g of distilled water for over 24 hours at 70°C under mechanical agitation with the aid of a magnetic stirrer bar, after which the extract was filtered. The carbon steel coupons studied have a simple chemical composition, with a weight percentage of 0.202% C, 0.161% Mn, 0.046% Cr, 0.035% P, 0.01% S, 0.007% Mo, 0.065% Si, with the remainder Fe as the base material. They were cut into discs of diameter 1 cm. The surface of the coupons was polished with 120, 400, 800, and 1500 grit emery papers. After grinding, the coupons were thoroughly washed with ethanol and water, followed by degreasing in acetone. Finally, the coupons were rinsed with distilled water before being dried with cool air. These pre-treated coupons were mounted in holders and immersed in the prepared corrosion solutions for testing. A 1 M HCl solution was used for the corrosion study. The FE solution was added into the corrosion solution at different concentration values of 0, 1, 3, 8, 12, 16 and 20 g/l.

2.2 Techniques

2.2.1 Surface analysis techniques

The surface morphology of the steel coupons and the composition of the inhibitor film formed on them were examined using FESEM coupled with EDX. The presence of functional groups which determine the nature of the inhibitors, such as organic or inorganic compounds present in the tested coupons were analysed by applying the FT-IR technique.

2.2.2 Electrochemical analysis

Dynamic polarization experiments were carried out using a potentiostat. The system comprises a three-electrode cell arrangement. A graphite road was used as the counter electrode, and saturated Calomel electrode was used as the reference electrode. The test coupons were used as the working electrode. A 250 ml volume of 1 M HCl solution, with the inhibitor added at the required concentration, was used for all corrosion experiments. The experiments were performed at temperatures ranging from 303 to 333 K under precisely controlled thermal conditions. The dynamic polarization experiment with a scan rate equal to 0.25 mV/s was conducted after 15 minutes of immersion, allowing a firm film to form on the metal surface. The applied potential ranging from -500 mV to +500. The EIS analysis involved applying an AC voltage with an amplitude of 10 mV at the open-circuit potential (OCP) over a frequency range from 100 kHz to 10 mHz. It was conducted within a conventional three-electrode cell setup, comprising a saturated Calomel electrode, platinum, and carbon steel coupon as reference, counter, and working electrodes, respectively. All electrochemical measurements were carried out using a CorrTest CS2350 potentiostat.

3. RESULTS AND DISCUSSION

3.1 Potentiodynamic Polarization Analysis

The Tafel plots in Fig. 1 show the electrochemical characteristics of carbon steel in 1 M HCl in the presence of different concentrations of the inhibitor FE and at different temperatures (303 K to 333 K). Table 1 gives the corresponding electrochemical parameters with important figures like corrosion current density (i_{corr}), corrosion potential (E_{corr}), Tafel slopes (β_c) and (β_a) for both cathodic and anodic reactions respectively. These parameters provide a full evaluation of the electrochemical performance and the inhibition ability of FE. From the experimental results, slightly different E_{corr} values with increasing concentration of FE are observed, suggesting that FE acts as an inhibitor of mixed type for both anodic and cathodic reactions. This kind of mechanistic behavior is consistent with previously published results on mixed-type corrosion inhibitors [29-32]. In addition, the results show a distinct temperature dependence of FE inhibition. Of note, the i_{corr} values decrease with temperature until an optimum value is reached and thereafter higher temperatures result in higher corrosion rate. This can be explained by a molecular rearrangement and/or partial decomposition of the inhibitor molecules at elevated temperatures, in accordance with a desorption mechanism which reduces their protection efficacy. The results obtained from experimental techniques were very consistent.

3.2 Corrosion inhibition efficiency

Corrosion current provides a good platform to determine the effectiveness of tested inhibitor for corrosion. However, the percentage of inhibition efficiency can simplify the evaluation of the reliability of the experimental data obtained. Inhibition efficiency I.E (%) was calculated using the following equation [32]:

$$\%IE = \frac{i_o - i_I}{i_o} \times 100 \quad (1)$$

where,

i_I : the corrosion current density of carbon steel in the presence of the inhibitor,

i_o : the corrosion current density of carbon steel in the absence of the inhibitor,

The results of the experimental data reported in Table 1 show that FE behaves as a corrosion inhibitor for carbon steel in 1 M HCl at different concentrations. The rate of inhibition decreases with increasing temperature. This reduction is attributed to a decrease of the adsorption of FE on the steel surface. The temperature-dependent trend suggests that the desorption of FE molecules and the possible roughening of the electrode surface may occur, both of which will accelerate the corrosion at a higher temperature [31,32]. Analysis of the efficiencies reveals that the optimum FE concentration is 16g/L at 303 K and the maximum inhibition efficiency is 87.2%. This result is in good agreement with known corrosion inhibition principles and demonstrates that FE works in these conditions. The agreement between the experimental results and theoretical expectations confirms the reliability of the employed methods of this research.

3.3 Characterization of FE

The FT-IR analysis was conducted to identify functional groups in the FE. As seen in Fig. 2, characteristic bands in the range of 3950- 3600 cm^{-1}, (i.e. the peaks 3901.6, 3861.82, 3843.41, 3649.45, 3664.61 cm^{-1}), indicate the presence of O-H stretching. The broadness suggests that the compound may contain hydrogen bonding. Around 2920-2850 cm^{-1}, (two peaks at 2923.72 and 2854.7) these peaks are associated with C-H stretching vibrations [33]. In the region around 1740 cm^{-1}, distinct peaks at 1868.31, 1798.87, and 1771.51 cm^{-1} are attributed to C=O stretching, commonly associated with carbonyl functional groups such as ketones or aldehydes [34].

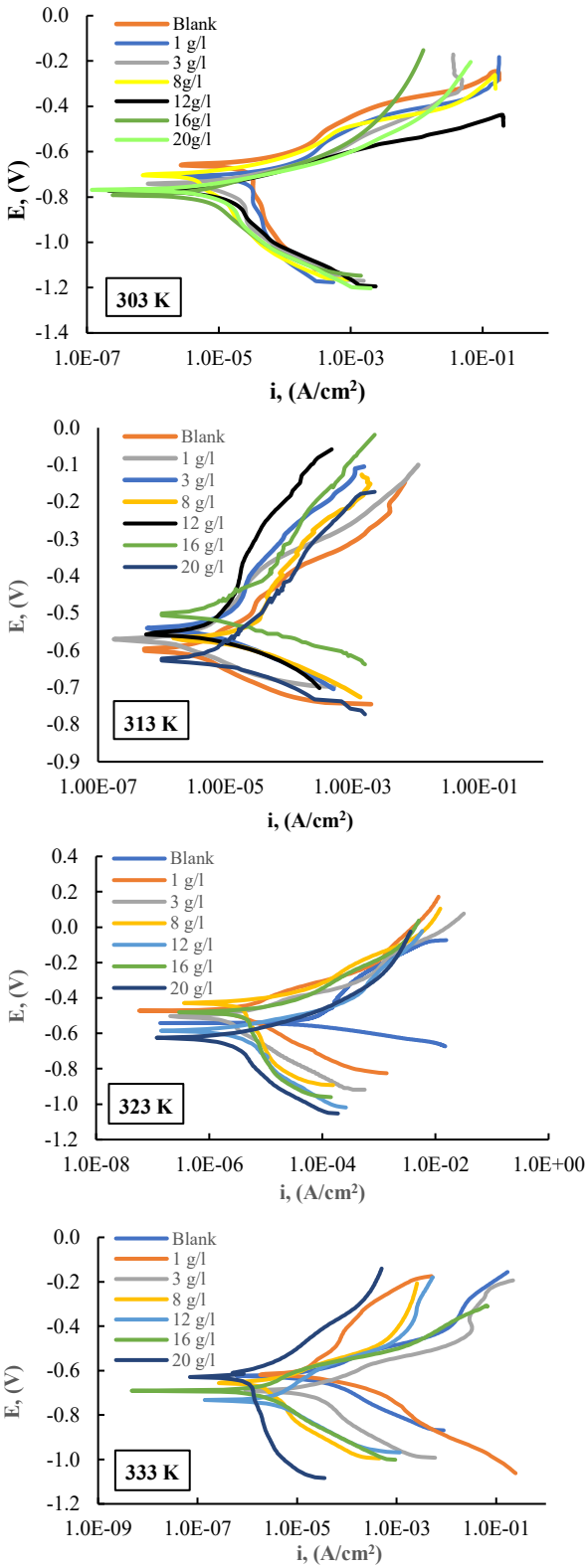

Figure 1. Tafel polarization plots for CS immersed in 1M HCl solution at different concentrations of FE and at different temperatures.

A peak at 1645.24 cm^{-1} falls within the 1650–1600 cm^{-1} range, suggesting C=C stretching, possibly due to aromatic or conjugated systems.

Additionally, multiple peaks between 1500 and 1400 cm^{-1} (1545.24, 1540.31, 1517.03, 1463.99, and 1417.57 cm^{-1}) align with C–H bending vibrations in aromatic compounds [34]. Peaks in the 1200–900 cm^{-1} range may be assigned to N–H_2 bending, C–H_2 deformation, and C–O stretching (e.g., ether linkages), while those between 850–600 cm^{-1} are consistent with CCO/COC vibrations and ring breathing modes [33-36].

These functional groups align well with the known chemical variability of frankincense resin, which—depending on species, geographic origin, and processing methods—typically contains monoterpenes, sesquiterpenes, diterpenes, triterpenes, polysaccharides, and essential oils [25,26]. Based on the spectral features and supported by previously reported literature [26-28], Table 2 shows a number of organic compounds likely present in the FE sample, considering the extraction and preparation conditions detailed in Section 2.1.

3.4 Electrochemical impedance spectroscopy analysis

The most frequently employed technique for evaluating corrosion behaviour is EIS, which offers valuable insights into the resistive and capacitive phenomena taking place at the metal-inhibitor interface [37]. Figure 3 represents the Nyquist and Bode plots of CS in 1M HCl solution without and with different concentrations of FE Inhibitor at 303 K.

Figure 3 shows the Nyquist plot, which relates the imaginary part of the impedance Z'' to its real part Z'. It is shown with enlarged semi-circles; a large capacitive loop at high frequencies and an inductive loop at low frequencies. The capacitive loop is representative of the charge-transfer resistance of charge-transfer processes between the steel surface and the surrounding solution. The inductive loop corresponds to relaxation effects due to H^+ ion adsorption or corrosion inhibitor species adsorption on the metal surface [38]. Without a corrosion inhibitor, a small inductive loop will create at low frequencies. This loop is attributed to generation of corrosion products at the metal surface, which leads to formation of an uneven electrode surface and a porous layer [39]. With the increase of FE inhibitor, the inductive loop is eliminated, which indicates the decrease of carbon steel corrosion [37].

Bode plots in Fig. 4 reveal a maximum, signifying that the corrosion of CS is predominantly regulated by the charge transfer resistance (Rp). Figure 4(a) demonstrates that impedance magnitude increases with an increase in inhibitor concentration over the entire frequency spectrum. These observations substantiate the adsorption of FE-based ionic liquid on the CS surface [36, 38]. Inhibition efficiency and Constant Phase Element (CPE) were computed utilizing the following Eq. 2 and 3, respectively [39].

$$\%IE = \left(\frac{R_P^{inh} - R_P}{R_P^{inh}}\right) \times 100 \quad (2)$$

$$Z_{CPE} = Q^{-1}(j\omega)^{-n} \quad (3)$$

Where R_P^{inh} and R_P represent the charge transfer resistance of the CS with and without the addition of FE, respectively. While Q represents the magnitude of the CPE. j is the imaginary number, ω denotes the angular frequency in rad/s, and n serves as the exponent of the CPE [37, 38].

Table 1: The Tafel plot polarization parameters at different FE concentrations and at different temperatures.

Concentration, (g/l)	β_a (mV/dec)	$-\beta_c$ (mV/dec)	i_{corr} (A/cm^2)	E_{corr} (V)	v (g/cm^2.h)	% I.E.	Θ (-)
			303 K				
Blank	156.85	11437	5.47E-05	-0.658	5.74E-05	-	-
1	104.14	4519.7	3.33E-05	-0.695	3.45E-05	39.2	0.39
3	111.53	1162.8	2.22E-05	-0.742	2.30E-05	59.5	0.60
8	96.032	551.41	1.42E-05	-0.722	1.46E-05	74.0	0.74
12	79.704	236.87	7.88E-06	-0.770	8.25E-06	85.6	0.86
16	106.19	259.51	7.00E-06	-0.790	7.31E-06	87.2	0.87
20	78.406	236.03	7.38E-06	-0.768	7.71E-06	86.5	0.86
			313 K				
Blank	235.3	17235.6	8.21E-05	-0.601	8.6E-05	-	-
1	160.4	6811.2	6.12E-05	-0.569	6.4E-05	25.4	0.25
3	160.4	1752.3	4.81E-05	-0.522	5.0E-05	41.3	0.41
8	126.9	831.0	3.61E-05	-0.571	3.8E-05	56.0	0.56
12	106.8	357.0	2.96E-05	-0.558	3.1E-05	63.9	0.64
16	133.9	391.1	2.53E-05	-0.506	2.6E-05	69.1	0.69
20	92.7	355.7	2.20E-05	-0.624	2.3E-05	73.2	0.73
			323 K				
Blank	99.447	10830.0	1.09E-04	-0.541	1.1E-04	-	-
1	83.604	14296.3	8.67E-05	-0.473	9.1E-05	20.7	0.21
3	84.790	9308.4	7.32E-05	-0.503	7.7E-05	33.1	0.33
8	90.018	10919.5	6.25E-05	-0.481	6.5E-05	42.9	0.43
12	83.996	12408.5	5.17E-05	-0.552	5.4E-05	52.7	0.53
16	79.343	11432.1	4.62E-05	-0.501	4.8E-05	57.7	0.58
20	72.1676	7022.0	3.76E-05	-0.624	3.9E-05	65.6	0.66
			333 K				
Blank	192.77	9207.53	1.48E-04	-0.616	1.5E-04	-	-
1	243.77	10072.47	1.29E-04	-0.633	1.3E-04	12.8	0.13
3	263.61	9679.46	1.14E-04	-0.628	1.2E-04	22.7	0.23
8	98.74	8535.44	9.94E-05	-0.606	1.0E-04	32.7	0.33
12	86.85	8095.24	8.64E-05	-0.723	9.0E-05	41.5	0.42
16	262.00	7847.88	7.95E-05	-0.691	8.3E-05	46.2	0.46
20	123.86	8108.260	7.40E-05	-0.638	7.7E-05	49.9	0.50

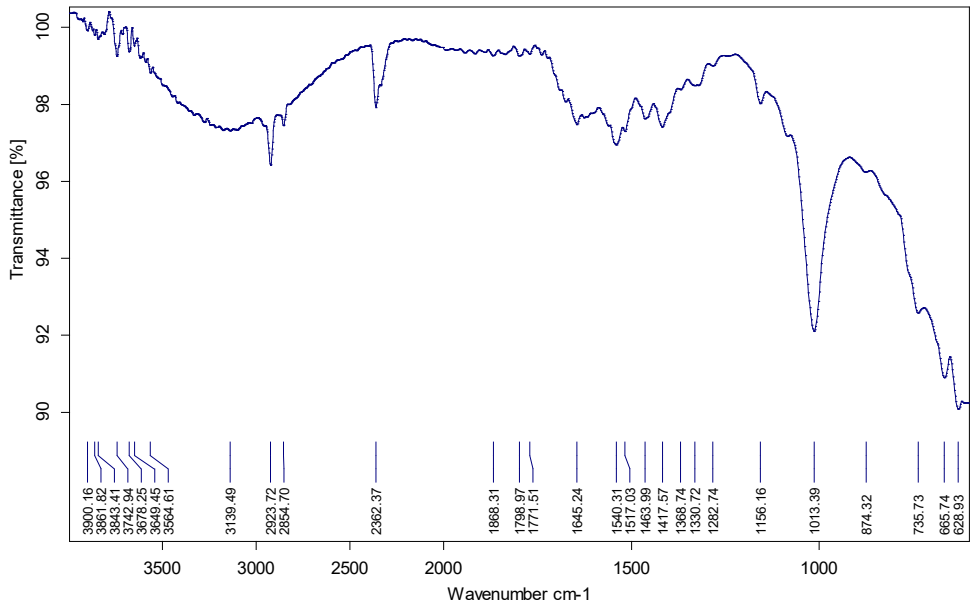

Figure 2. FT-IR spectra of FE.

Table 2: Organic compounds reported in literature as potential constituents of FE.

Category	Organic constituents
Short-chain organic acids	Acetic acid, Butyric acid, Valeric acid
Small alcohols	Linalool, Borneol, Terpinen-4-ol
Small aldehydes	Anisaldehyde, Cuminaldehyde
Phenols	Thymol, Eugenol
Heterocyclic compounds	Pyrazines

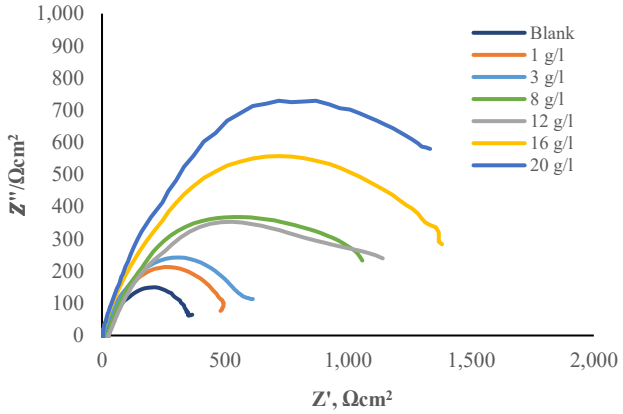

Figure 3. Nyquist plot of CS immersed in 1M HCl solution at different concentration of FE inhibitor and at 303 K.

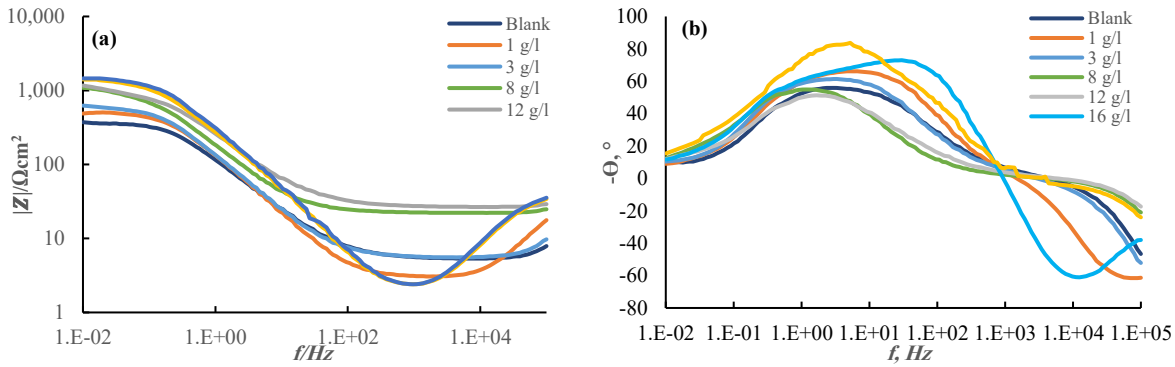

Figure 4. Bode plots of CS immersed in 1M HCl solution without and with different concentration of FE inhibitor and at 303K, (a) impedance |Z| vs. log *f* and (b) phase angle vs. log *f*.

Figure 5 employed an equivalent circuit model used for impedance analysis. The electrochemical impedance parameters, including R_s (solution resistance), R_p (charge transfer resistance), and CPE. The n value can be interpreted as an indicator of surface roughness or heterogeneity. When n equals 0, the CPE functions as a resistance, whereas n equals 1 signifies an ideal capacitor. The value of n, Q, and %IE (inhibition efficiency as a percentage), are presented in Table 3. The data in Table 3 reveals that R_p increased while CPE decreased with the rising concentration of FE. These findings suggest that inhibitor molecules are effectively adsorbed at the steel-solution interface. Additionally, the increase in n value with higher FE inhibitor concentrations indicates reduced surface inhomogeneity of steel, attributed to the adsorption of inhibitor molecules [38]. Furthermore, the inhibition efficiency reached its peak at 16 g/l. Specifically, in the 1M HCl solution, the %IE with FE concentration of 16 g/l was 75.89%. These findings indicate that the introduction of FE can effectively slow down the corrosion process.

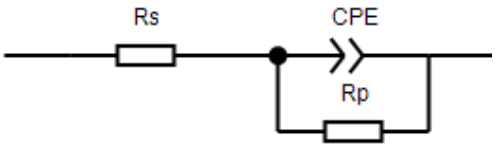

Figure 5. Equivalent circuit modelling of electrochemical impedance spectroscopy for carbon steel data in 1M HCl solution at different concentrations of FE inhibitor and at 303 K.

Table 3: Electrochemical impedance parameters of CS immersed in 1M HCl solution at different concentrations of FE and at 303 K.

Concentration, (g/l)	Rs (Ω.cm^2)	CPE-(Q) /cm^2	CPE-(n)	Rp (Ω.cm^2)	%IE
Blank	3.87	2.87×10^{-2}	0.61	376.38	0
1	9.66	2.61×10^{-2}	0.68	537.46	29.97
3	15.3	2.63×10^{-2}	0.71	653.02	42.36
8	22.06	8.83×10^{-2}	0.81	1231.5	69.44
12	26.93	4.87×10^{-2}	0.83	1392	72.96
16	36.81	6.98×10^{-2}	0.84	1560.9	75.89
20	35.25	6.65×10^{-2}	0.85	1526.8	75.62

3.5 Adsorption isotherm studies

The ability of organic molecules to adsorb onto metal surface is a standard criterion for evaluating the efficiency of corrosion inhibitors [40, 41]. The nature of the interaction between inhibitor molecules and the metal surface can be determined from the study of adsorption isotherms [40-43]. In the present work, the θ values calculated from the results of PDP technique, as detailed in Tables 1, were fitted to three adsorption isotherm models [42-44]:

Langmuir isotherm model:

$$\frac{C}{\theta} = \frac{1}{K_{ads}} + C \quad (4)$$

El-Awady isotherm model:

$$ln\frac{\theta}{1-\theta} = lnK_{ads} + ylnC \quad (5)$$

Temkin isotherm model:

$$\theta = \frac{1}{2\alpha}lnC - \frac{1}{2\alpha}lnb \quad (6)$$

where θ represents the degree of surface coverage of carbon steel by FE molecules. C is the concentration of the inhibitor FE in 1 M HCl solution, and K_{ads} is the adsorption equilibrium constant (l/g), which can be calculated from the intercepts of Eq. 4 and Eq. 5 plots. The symbol y denotes the number of water molecules displaced by one inhibitor molecule [42, 44]. The constant b represents the Temkin model constant, while α indicates the strength of the interaction between inhibitor molecules within the adsorbed layer; a negative value for α suggests the presence of repulsive forces, whereas a positive value indicates mutual attractive forces [41, 43].

The fitting results of the adsorption isotherms, presented in Fig. 6 and Table 4 confirmed that the adsorption of FE extract onto the steel surface in 1 M HCl solution across temperatures of 303–333K follows predominantly to the Langmuir model. In contrast, it did not conform well to the El-Awady and Temkin models. This suggests the formation of a monomolecular adsorbed layer devoid of significant intermolecular forces among the adsorbates [40-44].

Table 4: Langmuir adsorption model thermodynamic parameters for FE on CS at different temperatures.

T (K)	K_{ads} (l/g)	ΔG_{ads} (kJ/mol)	$-\Delta H_{ads}$ (kJ/mol)	$-\Delta S_{ads}$ (kJ/mol)
303	72.60	-30.745	42.526	0.041
313	39.60	-29.997		
323	26.40	-29.733		
333	17.60	-29.546		

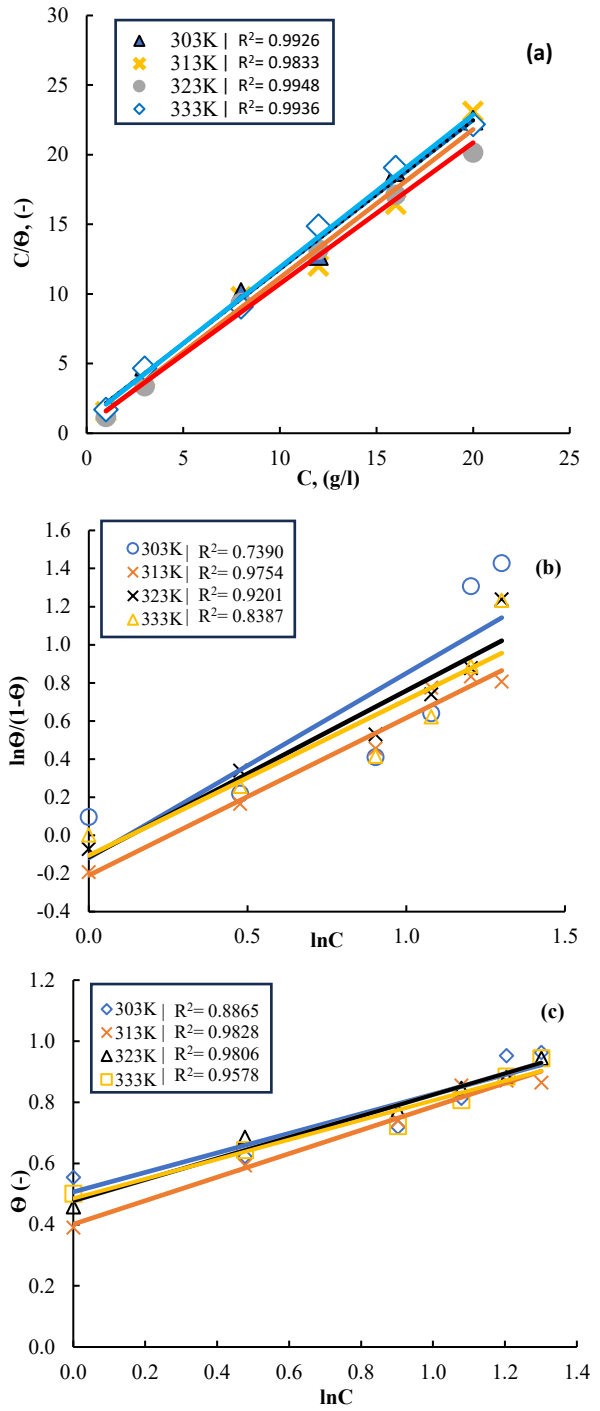

Figure 6. Adsorption isotherms of FE on CS, (a) Langmuir model, (b) El-Awady model, and (c) Temkin model.

The values of K_{ads} were calculated from the intercepts of the straight-lines plot of the Langmuir isotherm model. K_{ads} reflects the ability of inhibitor molecules to adsorb onto the CS surface [44, 45]. A higher K_{ads} value means a greater adsorption capacity of the inhibitor, leading to improved inhibition efficiency. As illustrated in Table 4, the K_{ads} values decreased significantly with rising solution temperature. Although the corrosion rate of steel increases at elevated temperatures, the capacity of the active molecules to adsorb onto the steel surface, i.e., θ, decreases. This confirms the increase in the inhibition efficiency of FE with rising temperature [40, 43, 45]. The calculations of adsorption thermodynamic parameters were done using the following Equations. [41, 44]:

$$\Delta G_{ads} = -RTln(\rho_{solution}K_{ads}) \quad (7)$$

$$\Delta G_{ads} = \Delta H_{ads} - T\Delta S_{ads} \quad (8)$$

$$ln(\rho_{solution}K_{ads}) = \left(-\frac{\Delta H_{ads}}{RT}\right) + \frac{\Delta S_{ads}}{R} \quad (9)$$

where, $\rho_{solution}$ is the density of solution and its equal to 962 g/l [44], R is a molar gas constant and T is the absolute temperature.

The Gibbs free energy values evaluated at different temperatures and inhibitor concentrations are negative signs and means that the inhibition process is feasible and spontaneous [44]. The development of an adsorbed protective film on the metal surface acts as a barrier, hindering both energy and mass transfer. As shown in Table 4, ΔG_{ads} values are negative and larger than -20 kJ/mol but less than -40 kJ/mol, which shows the feasibility of the FE inhibition process and signifies the mixed type of inhibition process. The thermodynamic parameters ΔH_{ads} and ΔS_{ads} were determined from the plot of Eq. 9, from the slope and intercept as shown in Fig. 7 yielding values of -42.526 kJ/mol and 0.041 kJ/mol·K, respectively. The negative enthalpy change signifies an exothermic adsorption process, consistent with the release of energy during the formation of a protective inhibitor layer on the metal surface. Based on the magnitude of ΔH_{ads} (≈ -40 kJ/mol), the adsorption mechanism is identified as predominantly physical adsorption. In contrast, enthalpy values exceeding 100 kJ/mol are typically associated with chemical adsorption processes. The positive value of ΔS_{ads} suggests a decrease in randomness at the solid-liquid interface during adsorption [44]. These results support a mixed physico-chemical inhibition mechanism and underscore the strong inhibitory efficacy of the FE extract.

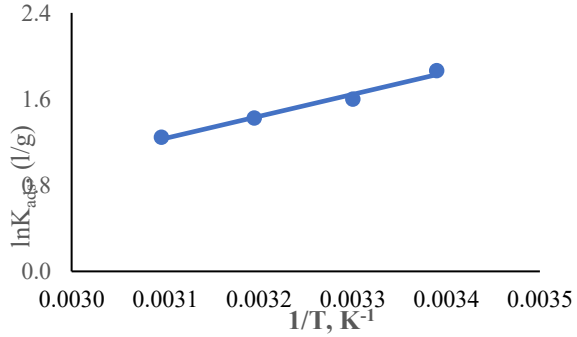

Figure 7. The plot of ln K_{ads} versus 1/T.

3.6 Adsorption kinetic studies

The evaluation of kinetic and thermodynamic parameters for the corrosion inhibition process is highly dependent on temperature. These parameters were determined using following the Arrhenius Eq. 10, and the transition state Eq. 11 [44, 45]:

$$lnv = lnA - \left(\frac{E_a}{RT}\right) \quad (10)$$

$$ln\left(\frac{v}{T}\right) = ln\left(\frac{R}{Nh}\right) + \left(\frac{\Delta S_a}{R}\right) - \left(\frac{\Delta H_a}{RT}\right) \quad (11)$$

where, v represent corrosion rate of CS, $v = \frac{Mi_{cor}}{nF}$, M is the relative atomic weight of CS, i.e. 56 g/mol, n is the number of exchange charges for the oxidation reaction of Fe, i.e. 2, F is the Faraday constant, i.e. 26.8 A.h.; E_a and A denoted activation energy and pre-exponential factor, respectively; R is molar gas constant; T is the adsorption temperature; h is Planck's constant, N is Avogadro's number; ΔG , ΔS_a, and ΔH_a are Gibbs free energy, entropy and enthalpy, respectively.

The plots of these two equations are presented in Fig. 8 at different concentrations of FE. The close alignment of the data points with the theoretical model underscores the consistency and reliability of the experimental results, thereby validating the applied methodology. A linear relationship was observed when lnv and $ln\left(\frac{v}{T}\right)$ were plotted against absolute temperature, yielding coefficient of determination (R^2) (an average value) of 0.996 and 0.983, respectively, and as illustrated in Figs. 8(a and b). The thermodynamic parameters are listed in Table 5. As shown in Table 5, The elevated activation energy observed in the presence of varying FE concentrations, compared to the uninhibited system, confirms the formation of an inhibitory complex layer on the CS surface [45, 47]. This increase in the energy barrier substantiates that corrosion inhibition via FE is thermodynamically favorable, as it impedes the metal dissolution process. The results align with prior reported studies [42-44] and adhere to the fundamental thermodynamic relation E_a - ΔH_a = RT, where the calculated values consistently exceed ΔH_a.

3.7 Surface morphology analysis

The FESEM images presented in Fig. 9 illustrate the surface morphology of CS coupons before (Fig. 9(a)) and after immersion in a 1M HCl solution, both without (Fig. 9(b)) and with the addition of 16 g/l of FE (Fig. 9(c)), over a period of 4 hours. In Fig. 9(b), it is evident that the CS surface exposed to the 1M HCl solution exhibits significant damage, likely attributed to the extensive dissolution of CS. Numerous cracks and pits are prominently distributed across the steel surface. Conversely, when 16 g/l of FE is introduced into the corrosive solution, as depicted in Fig. 9(c), a noticeable improvement in the appearance of the CS surface is observed. An inhibitor film is discernible on the CS surface, mitigating the dissolution of the CS and providing effective corrosion protection. The presence of this organic film, as observed in the FESEM images, corroborates the findings derived from the electrochemical measurements discussed in preceding sections.

The EDX analysis provided insights into the elemental composition of the CS surface, revealing the presence of Fe, O, and C. Interestingly, the CS coupon immersed in the solution without the inhibitor exhibited lower levels of iron, carbon, and oxygen content, which can be attributed to the corrosive nature of the solution. In contrast, the CS coupon immersed in the solution containing 16 g/l of the inhibitor displayed higher carbon and oxygen content, confirming the successful adsorption of inhibitor molecules onto the metal surface. The FE contains oxygen-rich functional groups, such as aromatic or heterocyclic rings, that can act as electron donors. Conversely, CS possesses vacant d-orbitals, making it an electron acceptor. This interaction results in a reduced corrosion rate. The presence of chlorine may be attributed to the formation of corrosion products containing chlorine or the adsorption of chloride ions onto the CS surface.

Table 5: Kinetics parameters of CS in 1M HCl at different FE concentrations.

Concentration, (g/l)	E_a (kJ/mol)	ΔH (kJ/mol)	$-\Delta S$ (J/mol)
Blank	127.89	125.24	110.7
1	133.29	130.64	150.2
3	148.51	145.86	182.0
8	148.41	145.76	187. 9
12	157.63	154.98	188.6
16	148.58	145.93	196.2
20	159.73	157.08	216.2

3.8 Quantum chemical calculations

The present study used Density Functional Theory (DFT) to investigate the adsorption behavior of FE constituents onto a metal surface and to establish a relation between molecular structure and inhibition efficiency. All computations were performed using ArgusLab software (version 4.0.1) [48-50]. Although molecular optimization was feasible for both gas and aqueous phases, the calculations were performed to the solution phase due to the electrochemical nature of the corrosion process targeted by inhibitors. Consequently, a comprehensive set of electronic properties was determined in solution, including: the

highest occupied molecular orbital (HOMO), the lowest unoccupied molecular orbital (LUMO), the energy gap (ΔE), ionization potential (I), electron affinity (A), dipole moment (μ), electronegativity (χ), absolute hardness (η), softness (σ), and the fraction of electron transfer (ΔN) [48, 51]. The selection of these water-soluble compounds for detailed modelling was based on their potential to act as electron donors. The specific constituents subjected to this quantum chemical analysis are listed in Table 5, which aims to elucidate their adsorption and inhibition mechanisms.

3.9 Quantum chemical calculations

The present study used Density Functional Theory (DFT) to investigate the adsorption behavior of FE constituents onto a metal surface and to establish a relation between molecular structure and inhibition efficiency. All computations were performed using ArgusLab software (version 4.0.1) [48-50]. Although molecular optimization was feasible for both gas and aqueous phases, the calculations were performed to the solution phase due to the electrochemical nature of the corrosion process targeted by inhibitors. Consequently, a comprehensive set of electronic properties was determined in solution, including: the highest occupied molecular orbital (HOMO), the lowest unoccupied molecular orbital (LUMO), the energy gap (ΔE), ionization potential (I), electron affinity (A), dipole moment (μ), electronegativity (χ), absolute hardness (η), softness (σ), and the fraction of electron transfer (ΔN) [48, 51]. The selection of these water-soluble compounds for detailed modelling was based on their potential to act as electron donors. The specific constituents subjected to this quantum chemical analysis are listed in Table 6, which aims to elucidate their adsorption and inhibition mechanisms.

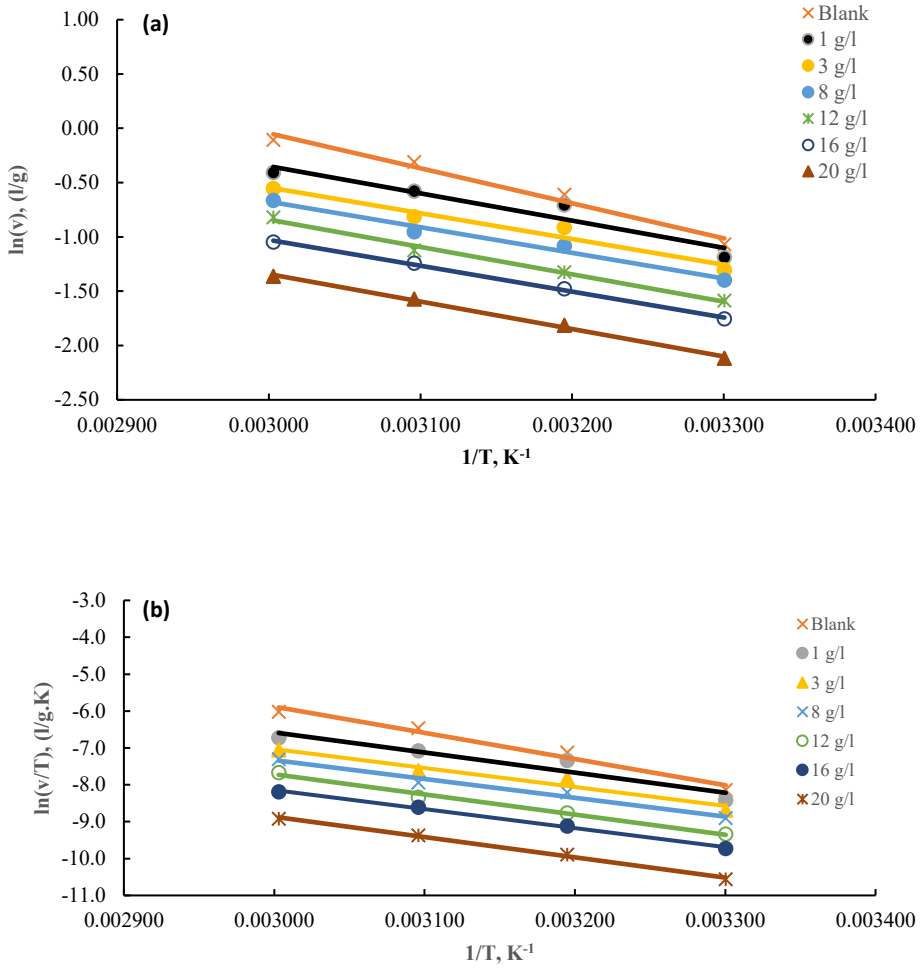

Figure 8. Fitting lines for the adsorption kinetic equations of CS in 1M HCl solution at different FE concentrations: (a) Arrhenius equation, and (b)Transition- state equation.

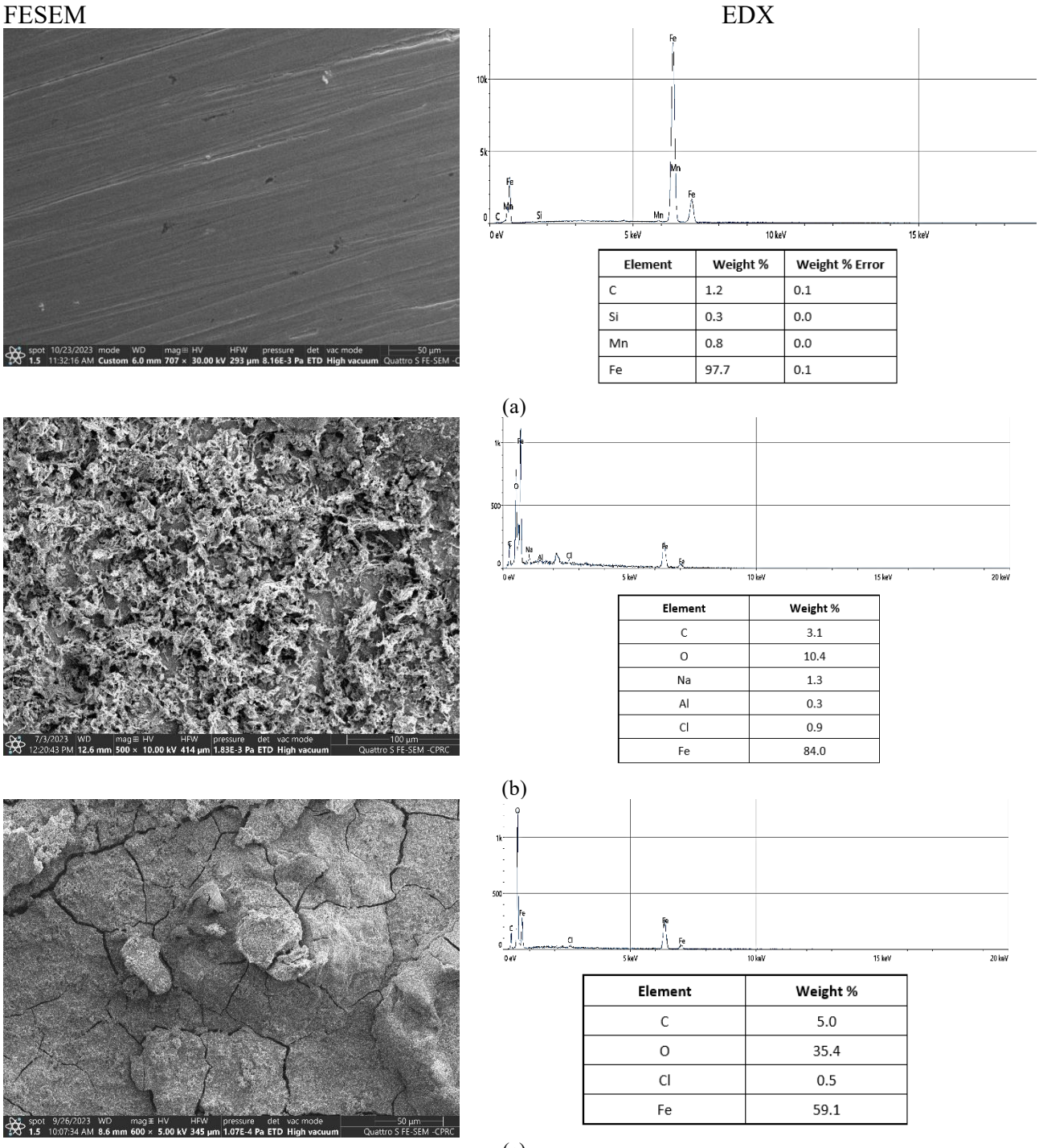

Element	Weight %	Weight % Error
C	1.2	0.1
Si	0.3	0.0
Mn	0.8	0.0
Fe	97.7	0.1

Element	Weight %
C	3.1
O	10.4
Na	1.3
Al	0.3
Cl	0.9
Fe	84.0

Element	Weight %
C	5.0
O	35.4
Cl	0.5
Fe	59.1

Figure 9. FESEM and EDX spectra images of CS (a) before immersion (b) after immersion (c) after immersion and addition of 16g/l FE at 303 K.

3.10 Quantum chemical calculations

The present study used Density Functional Theory (DFT) to investigate the adsorption behavior of FE constituents onto a metal surface and to establish a relation between molecular structure and inhibition efficiency. All computations were performed using ArgusLab software (version 4.0.1) [48-50]. Although molecular optimization was feasible for both gas and aqueous phases, the calculations were performed to the solution phase due to the electrochemical nature of the corrosion process targeted by inhibitors. Consequently, a comprehensive set of electronic properties was determined in solution, including: the highest occupied molecular orbital (HOMO), the lowest unoccupied molecular orbital (LUMO), the energy gap (ΔE), ionization potential (I), electron affinity (A), dipole moment (μ), electronegativity (χ), absolute hardness (η), softness (σ), and the fraction of

electron transfer (ΔN) [48, 51]. The selection of these water-soluble compounds for detailed modelling was based on their potential to act as electron donors. The specific constituents subjected to this quantum chemical analysis are listed in Table 5, which aims to elucidate their adsorption and inhibition mechanisms.

Table 6: Organic compounds used for quantum chemical calculations.

Category	Organic compound
Short-chain organic acids	Valeric acid
Short-chain alcohols	Terpinen-4-ol
Short-chain aldehydes	Cuminaldehyde
Phenols	Eugenol
Heterocyclic compounds	2,5-Dimethylpyrazine

Table 7: Quantum chemical parameters of FE.

Compound	E_{HOMO} (eV)	E_{LUMO} (eV)	ΔE (eV)	Ionization potential (I)	Electron affinity (A)	μ (Debye)	χ (eV)	η (eV)	σ (eV^{-1})	ΔN
Cuminaldehyde	-8.45	-0.65	7.80	8.45	0.65	6.0	4.55	3.90	0.256	1.167
Eugenol	-7.70	+0.30	8.00	7.70	-0.30	5.1	3.70	4.00	0.250	0.925
Valeric Acid	-8.85	-0.65	8.20	8.85	0.65	4.5	4.75	4.10	0.244	1.159
2,5-Dimethylpyrazine	-8.30	+0.05	8.35	8.30	-0.05	5.8	4.13	4.18	0.239	0.988
Terpinen-4-ol	-8.05	+0.55	8.50	8.05	-0.55	4.2	3.75	4.30	0.233	0.872

Figure 10 presents the optimized structures of the FE inhibitor constituents under investigation. Computed quantum chemical parameters are tabulated in Table 7. The HOMO and LUMO densities are predominantly localized on heteroatoms, aromatic rings, carbonyls and hydroxyls (Fig. 10), indicating these regions serve as primary adsorption sites. Inhibitor molecules adsorb onto the metal surface through donor-acceptor interactions involving π-electrons of the inhibitor and vacant d-orbitals of carbon steel surface [51, 52].

The E_{HOMO} energy governs electron donation to electrophilic metal surfaces. The higher the value the more inhibitor molecule tendency to donate electrons to acceptor molecule, as a result, the inhibition efficiency increases due to the adsorption of inhibitor molecule on carbon steel surface. In contrast, the lower value of E_{HOMO} values express the inhibitor molecule ability to accept electrons from the carbon steel surface. The more efficient inhibitors are those molecules that offer electrons to LUMO as well as accept electrons from CS surface [53, 54]. Effective corrosion inhibitors exhibit dual functionality: electron donation to metal orbitals and acceptance of electrons from metallic surfaces. The energy gap ($\Delta E=E_{HOMO}-E_{LUMO}$) value directly corresponds to enhanced inhibitory performance, due to facilitating electron transfer mechanisms at the metal-electrolyte interface predicts molecular stability and reactivity [12]. A smaller value of ΔE shows high inhibition efficacy as low energy gap represents high reactivity of molecules toward metal surface hence enhancement of adsorption process occurs [50].

The results indicate that cuminaldehyde has the lowest energy gap (ΔE = 7.80 eV) among FE constituents, which means that it is slightly more reactive than other compounds and will adsorb on the CS surface. Although the calculated values of ΔE, for the key FE components are close to each other, the values are in the following order: Cuminaldehyde < Eugenol < Valeric Acid < 2,5-Dimethylpyrazine < Terpinen-4-ol. However, there is a minor increase in chemical reactivity associated with this minor change. Besides, electronegativity principle states the tendency of electrons to transfer from a species with lower χ to that with higher χ until the chemical potentials are compensated [54, 55].

In conceptual DFT, the absolute hardness (η) is an important descriptor of molecular stability and reactivity. Generally, the energy levels of such molecules are high enough and the energy gaps are wide enough to render the molecule relatively inert, namely, if the molecule's hardness is high, its polarizability is low and also its electron-donating and its reactive properties are both less. Low molecular weight organic compounds with low molecular weight and narrow energy gap are more reactive with high electron donating ability and lower entropy. This hardness-softness classification is useful for predicting the interaction between the molecules, particularly in the adsorption mechanism concerning corrosion inhibition [49, 50].

The dipole moment (μ) also has a big part in the adsorption of inhibitor molecules at metal surfaces [48]. Increase of the μ is associated with a stronger electrostatic interaction and a better surface coverage and inhibition performance [52]. Another important DFT parameter is the degree of electron transfer (ΔN) which indicates the strength of the electron donation ability of an inhibitor towards the metal. The resulting change in ΔN, can be found as follows [52]:

$$\Delta N = \frac{\chi_{Fe}-\chi_{inh}}{2(\eta_{Fe}-\eta_{inh})} \quad (12)$$

where χ = electronegativity, η: is the absolute hardness of the metal and the inhibitor. If the ΔN is

positive then there is electron transfer from the inhibitor to the metal which indicates strong adsorption of the inhibitor and effective inhibition. Using parameters of Fe: direction of magnetization of Fe, which is 7 eV, and the spin exchange energy of Fe, which is 0 eV mol^{-1}, the parameters of the inhibitor are given by [54]:

$$\chi_{inh} = \frac{(I+A)}{2} = -\frac{(E_{HOMO}+E_{LUMO})}{2} \quad (13)$$

$$\eta_{inh} = \frac{(I-A)}{2} = -\frac{(E_{HOMO}-E_{LUMO})}{2} \quad (14)$$

The obtained values of the ΔN ($0 < \Delta N < 3.6$) demonstrate the favourable electron-donating capacity of the used FE constituents facilitating their adsorption on the metal surface. The compounds can be arranged according to their electron donating ability in the order of cuminaldehyde > valeric acid > 2,5-dimethylpyrazine > eugenol > terpinen-4-ol.

3.11 Mechanism of corrosion inhibition

The adsorption mechanism of the FE constituents onto the CS surface, as revealed by the quantum chemical calculations, involves a combination of physisorption and chemisorption. The calculated free energy of adsorption for FE ($-20 < \Delta G_{ads} < -40$ kJ/mole) supports this mixed-mode mechanism [50]. The inhibitory action is primarily driven by the electron-donating ability of heteroatoms (N, O) and functional groups (carbonyl, hydroxyl), as indicated by the HOMO localization and the positive ΔN values (Table 7).

The inhibitory efficacy of FE is attributed to its molecular adsorption, which is facilitated by the presence of electron-donating heteroatoms, specifically nitrogen and oxygen, within its structure. This adsorption behavior can be interpreted through the HOMO-LUMO or the Hard and Soft Acids and Bases (HSAB) principle [52]. According to the former, lone electron pairs located on heteroatoms, carbonyl, and hydroxyl group which constitute the highest HOMO can form coordinate covalent bonds with vacant d-orbitals of iron atoms on the surface. This electron donation leads to an accumulation of negative charge on the metal, which is subsequently stabilized by back-donation of electrons from the metal to the antibonding π* orbital (LUMO) of the inhibitor molecule. This synergistic donor-acceptor interaction enhances the stability of the adsorbed layer and strengthens the binding affinity between the inhibitor and the active metal sites [54]. Also, complementing this view, the HSAB principle posits that stable complexes form between soft acids and soft bases or hard acids and hard bases. In this context, the iron surface, with its vacant d-orbitals, acts as a soft acid, while the electron-rich heteroatoms of the inhibitor molecule function as a soft base. Their mutual interaction, as predicted by the HSAB principle, results in effective adsorption [54, 55].

Furthermore, the formation of a stable iron-inhibitor complex on the metal surface can reduce the solubility of the protective layer and physically block active sites, thereby hindering the metal dissolution process and diminishing the overall corrosion rate [50-55]. A proposed mechanism for the corrosion inhibition of CS by FE is illustrated in Fig. 11.

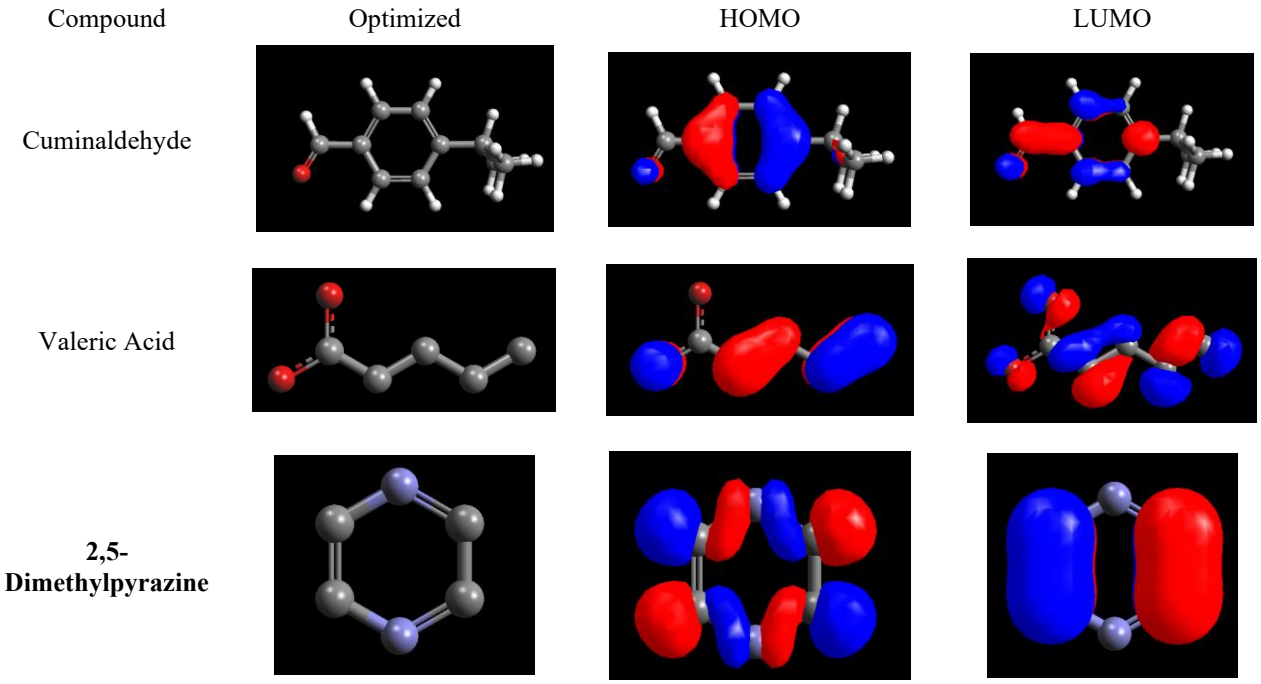

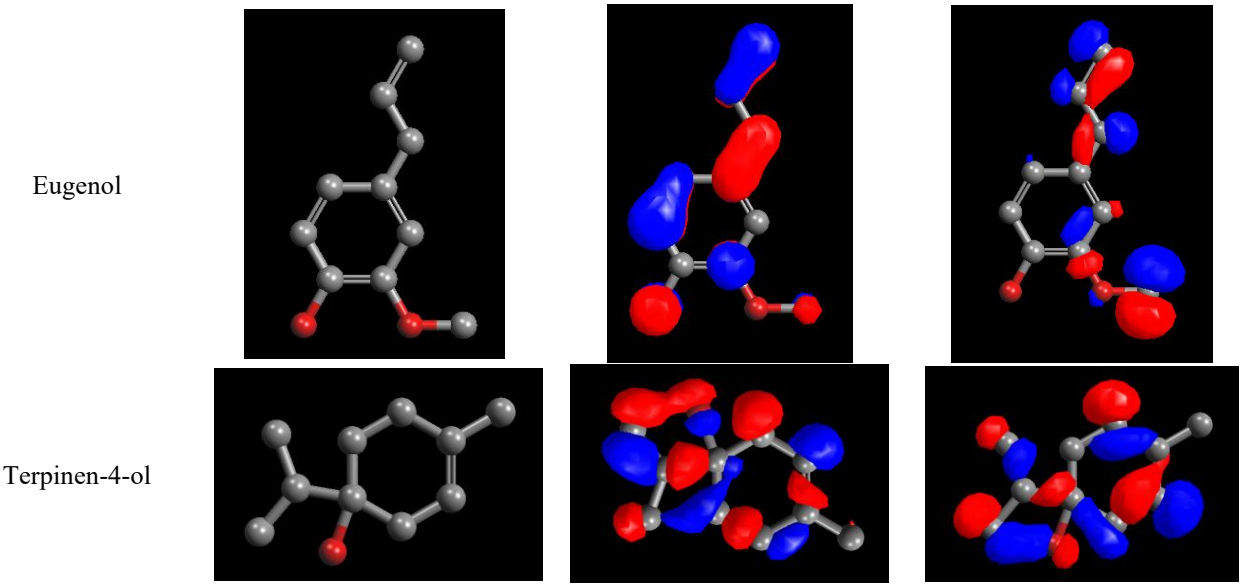

Figure 10. Optimized structures, HOMO and LUMO energies of protonated form of Cuminaldehyde, Valeric Acid, 2,5-Dimethylpyrazine, Eugenol and Terpinen-4-ol**.**

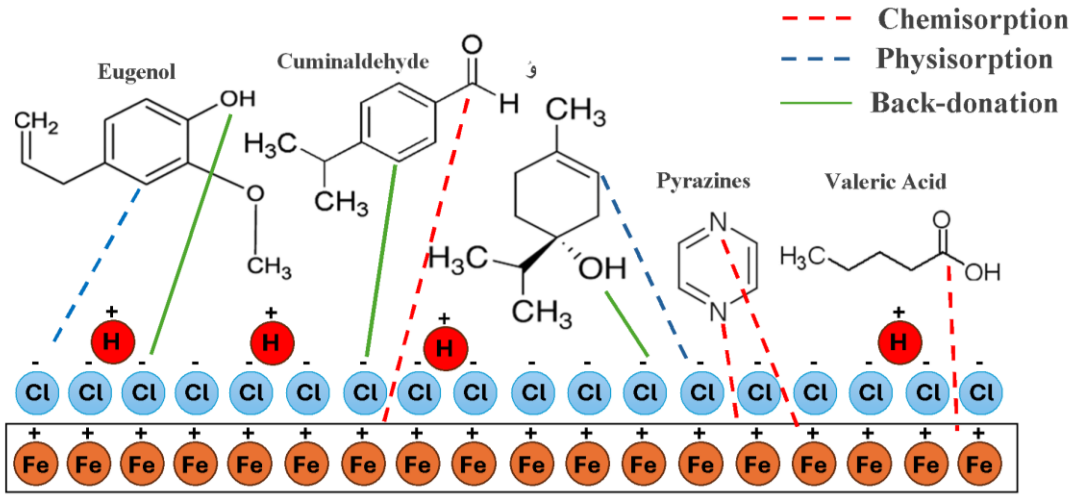

Figure 11. Schematic diagram of the adsorption mechanism of FE molecules on the CS surface in 1 M HCl solution.

4. CONCLUSION

The anti-corrosive performance of a natural extract (FE) on carbon steel in 1 M HCl was comprehensively investigated using electrochemical methods and surface characterization techniques. The following specific conclusions were derived from experimental and theoretical analyses:

1- FE exhibited remarkable corrosion inhibition capabilities, with efficiency positively correlated to concentration and inversely related to temperature. Maximum inhibition efficiency of 87.2% was achieved at 16 g/l and 303K.
2- PDP studies confirmed the mixed-type inhibition behavior of FE, with remarkedly influence on both anodic and cathodic sites on the metal.
3- Adsorption mechanism analysis established that FE constituents follow the Langmuir adsorption isotherm model, suggesting monolayer coverage through combined physiochemical interactions at the metal-solution interface.
4- Surface characterization techniques, including FESEM/EDX spectroscopy, and FTIR spectroscopy, provided unequivocal evidence of protective film formation, surface morphology modification, and substantial reduction in corrosion-induced surface degradation.
5- Quantum chemical computations and adsorption free energy calculations revealed dual adsorption mechanisms involving both physisorption and chemisorption, with physical adsorption interactions predominating the protective process.

6- This research establishes FE as an environmentally benign, economically viable, and technically efficient corrosion inhibition alternative that provides multifunctional protection for carbon steel infrastructures in aggressive acidic environments.

REFERENCES

[1] C. P. Mungwari, B. A. Obadele, and C. K. King'ondu, "Phytochemicals as green and sustainable corrosion inhibitors for mild steel and aluminium: Review," *Results in Surfaces and Interfaces*, vol. 18, p. 100374, 2025, doi: 10.1016/j.rsurfi.2024.100374.

[2] P. Kumar et al., "Advancements in ionic liquid-based corrosion inhibitors for sustainable protection strategies: From experimental to computational insights," *Advances in Colloid and Interface Science*, vol. 333, p. 103303, 2024, doi: 10.1016/j.cis.2024.103303.

[3] A. Al-Amiery, W. N. R. Wan Isahak, and W. K. Al-Azzawi, "Sustainable corrosion inhibitors: A key step towards environmentally responsible corrosion control," *Ain Shams Engineering Journal*, vol. 15, no. 5, p. 102672, 2024, doi: 10.1016/j.asej.2024.102672.

[4] P. D. A. Bastos et al., "A corrosion evaluation of mild carbon steel in reclaimed refinery stripped sour water," *J. Environ. Manage.*, vol. 272, p. 111080, 2020, doi: 10.1016/j.jenvman.2020. 111080.

[5] S. Karthick, S. Muralidharan, and V. Saraswathy, "Corrosion performance of mild steel and galvanized iron in clay soil environment," *Arabian J. Chem.*, vol. 13, no. 1, pp. 3301–3318, 2020, doi: 10.1016/j.arabjc. 2018.11.005.

[6] Palli, S., Majhi, J. & Raja, V.S. Development of an Efficient Acid Pickling Bath for Hot-Rolled Steel Coil. Trans Indian Inst Met 75, 1781–1788 (2022). doi.org/10.1007/s12666-022-02556-y.

[7] Xie, Q., Shi, Py., Liu, Cj. et al. Effects of Different Oxidants on HCl-based Pickling Process of 430 Stainless Steel. J. Iron Steel Res. Int. 23, 778–783 (2016). doi.org/10.1016/S1006-706X(16)30120-0.

[8] Hanaa M. Elabbasy, Ahmed A. El-Sherbini, Abd Elaziz S. Fouda, Ricinus communis leaves extract as a green corrosion inhibitor for carbon steel in hydrochloric acid solution, Journal of the Indian Chemical Society, Volume 101, Issue 12, 2024, 101491, doi.org/10.1016/j.jics.2024. 101491.

[9] Atmane Djermoune, Radouane Maizia, Moussa Zahzouh, Youcef Khelfaoui, Aloysia triphylla plant extract as an eco-friendly corrosion inhibitor for API 5L X42 steel in hydrochloric acid medium: A combined experimental and DFT study, Colloids and Surfaces A: Physicochemical and Engineering Aspects, Volume 709, Part 1, 2025, 136068, doi.org/10.1016/j.colsurfa.2024.136068.

[10] Houaria Derfouf, Boulanouar Messaoudi, Tarik Attar, M'hamed Guezzoul, Wan Jefrey Basirun, Experimental and theoretical study of Atriplex halimus L. leaves extract as an ecologic corrosion inhibitor for XC38 carbon steel in an HCl environment, Journal of Molecular Liquids, Volume 433, 2025, 127785, doi.org/10.1016/j. molliq.2025.127785.

[11] K. O. Sulaiman, A. T. Onawole, O. Faye, and D. T. Shuaib, "Understanding the corrosion inhibition of mild steel by selected green compounds using chemical quantum based assessments and molecular dynamics simulations," *J. Mol. Liq.*, vol. 279, pp. 342–350, 2019.

[12] H. Thacker and V. Ram, "Green corrosion inhibitors derived from plant extracts and drugs for mild steel in acid media: A review," *Results in Surfaces and Interfaces*, vol. 18, p. 100364, 2025, doi: 10.1016/j.rsurfi.2024.100364.

[13] Y. Li et al., "Exploring the potential of plant extracts as corrosion inhibitors: A comprehensive review," *Prog. Org. Coat.*, vol. 198, p. 108915, 2025, doi: 10.1016/j.porgcoat. 2024.108915.

[14] G. P. V. Dalmora et al., "Methods of corrosion prevention for steel in marine environments: A review," *Results in Surfaces and Interfaces*, p. 100430, 2025, doi: 10.1016/j.rsurfi.2025. 100430.

[15] Bandeira, R.M., Lima, F.P., Nunes, M.S. et al. The green plant-based corrosion inhibitors—a sustainable strategy for corrosion protection. Surf. Sci. Technol. 3, 19 (2025). doi.org/10.1007/ s44251-025-00084-7.

[16] Jaddoa, H.A., Ali, J.M. & Abdulhussein, B.A. A Review of Corrosion Inhibition of Carbon Steel Using Fruit, Vegetable and Rice Husk Extract. Russ J Appl Chem 97, 134–146 (2024). doi.org/10.1134/S1070427224010117.

[17]Tabyaoui, M., Tourabi, M., Zarrok, H. et al. Citrullus colocynthis fruit extract as effective eco-friendly corrosion inhibitor in a hydrochloric acid pickling medium for carbon steel by using both experimental and theoretical studies. Environ Sci Pollut Res 31, 43757–43780 (2024). doi.org/10.1007/s11356-024-34055-6.

[18] Radouane Maizia, Atmane Djermoune, Damia Amoura, Aida Zaabar, Anthony Thomas, Abdelhafid Dib, Serguei Martemianov, Bidens aurea aiton plant extract as a green and sustainable corrosion inhibitor for carbon steel X42 in hydrochloric acidic medium: Experimental and computational studies, Materials Chemistry and Physics, Volume 339, 2025, 130740, doi.org/10.1016/j.matchemphys.2025.130740.

[19] Hala. M. Hassan, Potentilla erecta extract as a green and eco-friendly corrosion inhibitor for 360 carbon steel in hydrochloric acid environment, International Journal of Electrochemical Science, Volume 20, Issue 6, 2025, 101028, doi.org/10.1016/j.ijoes.2025. 101028.

[20] Qahtan A. Yousif, Mahmoud A. Bedair, Ahmed M. Abuelela, Azaj Ansari, Sumit Sahil Malhotra, Zainb Fadel, High-performance corrosion inhibitors for carbon steel in hydrochloric acid: electrochemical and DFT studies, RSC Advances, Volume 15, Issue 35, 2025, Pages 28666-28688, doi.org/10.1039/d5ra04952k.

[21] Khang Duy Huu Nguyen, Tran Dinh Manh, Lien Thi Phuong Nguyen, Dao Thanh Vu, Kim Long Duong Ngo, Syzygium polyanthum (Wight) Walp. leaf extract as a sustainable corrosion inhibitor for carbon steel in hydrochloric acidic environment, Journal of Industrial and Engineering Chemistry, Volume 143, 2025, Pages 468-487, doi.org/10.1016/j.jiec. 2024.08.054.

[22] Florez-Frias EA, Barba V, Lopez-Sesenes R, Landeros-Martínez LL, los Ríos JPF-D, Casales M et al (2021) Use of a metallic complex derived from Curcuma longa as green corrosion inhibitor for carbon steel in sulfuric acid. Int J Corros 2021:6695299. doi.org/10.1155/2021/6695299.

[23] A. Singh, E. E. Ebenso, and M. A. Quraishi, "Corrosion Inhibition of Carbon Steel in HCl Solution by Some Plant Extracts," International Journal of Corrosion, vol. 2012, pp. 1–20, 2012, doi.org/10.1155/2012/897430.

[24] Chigondo, M., Chigondo, F. Recent natural corrosion inhibitors for mild steel: an overview. J. Chem. 2016; doi.org/10.1155/2016/6208937.

[25] Hussain, H.; Rashan, L.; Hassan, U.; Abbas, M.; Hakkim, F.L.; Green, I.R. Frankincense diterpenes as a bio-source for drug discovery. Expert Opin. Drug Discov. 2022, 17,513–529. doi.org/10.1080/ 17460441.2022.2044782.

[26] Thomas Efferth, Franz Oesch, Anti-inflammatory and anti-cancer activities of frankincense: Targets, treatments and toxicities, Seminars in Cancer Biology, Volume 80, 2022, Pages 39-57, doi.org/10.1016/j.semcancer. 2020.01.015.

[27] Rafie Hamidpour, Soheila Hamidpour, Mohsen Hamidpour, Mina Shahlari, Frankincense (乳香 Rǔ Xiāng; Boswellia Species): From the Selection of Traditional Applications to the Novel Phytotherapy for the Prevention and Treatment of Serious Diseases, Journal of Traditional and Complementary Medicine, Volume 3, Issue 4, 2013, Pages 221-226, doi.org/10.4103/2225-4110.119723.

[28] Abuzar Kabir, Francesco Cacciagrano, Angela Tartaglia, Marica Lipsi, Halil Ibrahim Ulusoy, Marcello Locatelli, Chapter 7 - Analysis of monoterpenes and monoterpenoids, Editor(s): Ana Sanches Silva, Seyed Fazel Nabavi, Mina Saeedi, Seyed Mohammad Nabavi, Recent Advances in Natural Products Analysis, Elsevier, 2020, Pages 274-286, ISBN 9780128164556, doi.org/10.1016/B978-0-12-816455-6.00007-X.

[29] A. Dehghani et al., "A combined experimental and theoretical study of green corrosion inhibition of mild steel in HCl solution by aqueous Citrullus lanatus fruit (CLF) extract," *J. Mol. Liq.*, vol. 279, pp. 603–624, 2019, doi: 10.1016/j.molliq. 2019.02.010.

[30] Z. Zhang, H. Ba, and Z. Wu, "Sustainable corrosion inhibitor for steel in simulated concrete pore solution by maize gluten meal extract: Electrochemical and adsorption behavior studies," *Constr. Build. Mater.*, vol. 227, 2019, doi: 10.1016/j.conbuildmat. 2019.117080.

[31] K. Azzaoui et al., "Eco-friendly green inhibitor Gum Arabic (GA) for the corrosion control of mild steel in hydrochloric acid medium," *Corros. Sci.*, vol. 129, pp. 70–81, 2017, doi: 10.1016/j.corsci.2017.09.027.

[32] A. Pradityana et al., "Inhibition of corrosion of carbon steel in 3.5% NaCl solution by Myrmecodia Pendans extract," *Int. J. Corros.*, vol. 2016, pp. 1–6, 2016, doi: 10.1155/2016/ 6058286.

[33] A. Dehghani, G. Bahlakeh, B. Ramezanzadeh, and M. Ramezanzadeh, "Potential of Borage flower aqueous extract as an environmentally sustainable corrosion inhibitor for acid corrosion of mild steel: Electrochemical and theoretical studies," *J. Mol. Liq.*, vol. 277, pp. 895–911, 2019.

[34] B. Tan et al., "Papaya leaves extract as a novel eco-friendly corrosion inhibitor for Cu in H_2SO_4 medium," *J. Colloid Interface Sci.*, vol. 582, pp. 918–931, 2021.

[35] E. de Britto Policarpi and A. Spinelli, "Application of Hymenaea stigonocarpa fruit shell extract as eco-friendly corrosion inhibitor for steel in sulfuric acid," *J. Taiwan Inst. Chem. Eng.*, vol. 116, pp. 215–222, 2020.

[36] M. Keramatinia, B. Ramezanzadeh, and M. Mahdavian, "Green production of bioactive components from herbal origins through one-pot oxidation/polymerization reactions and application as a corrosion inhibitor for mild steel in HCl solution," *J. Taiwan Inst. Chem. Eng.*, vol. 105, pp. 134–149, 2019.

[37] T. Tüken et al., "Inhibition effect of 1-ethyl-3-methylimidazolium dicyanamide against steel corrosion," *Corros. Sci.*, vol. 59, pp. 110–118, 2012.

[38] R. S. Erami et al., "Carboxamide derivatives as new corrosion inhibitors for mild steel protection in hydrochloric acid solution," *Corros. Sci.*, vol. 151, pp. 190–197, 2019, doi: 10.1016/j.corsci. 2019.02.019.

[39] Y. Qiang, S. Zhang, and L. Wang, "Understanding the adsorption and anticorrosive mechanism of DNA inhibitor for copper in sulfuric acid," *Appl. Surf. Sci.*, vol. 492, pp. 228–238, 2019.

[40] Ali Zakeri, Elnaz Bahmani, Alireza Sabour Rouh Aghdam, Plant extracts as sustainable and green corrosion inhibitors for protection of ferrous metals in corrosive media: A mini review, Corrosion Communications, Volume 5, 2022, Pages 25-38.

[41] O.D. Onukwuli, I.A. Nnanwube, F.O. Ochili, M. Omotioma, DFT, experimental and optimization studies on the corrosion inhibition of aluminium in H2SO4 with danacid as inhibitor, Results in Engineering, Volume 24, 2024, 103113, doi.org/10.1016/j.rineng.2024.103113.

[42] Olatunde Alaba Akinbulumo, Oludare Johnson Odejobi, Ebenezer Leke Odekanle, Thermodynamics and adsorption study of the corrosion inhibition of mild steel by Euphorbia heterophylla L. extract in 1.5 M HCl, Results in Materials, Volume 5, 2020, 100074.

[43] Priya Vashishth, Himanshi Bairagi, Rajni Narang, Sudhish K. Shukla, Lukman O. Olasunkanmi, Eno E. Ebenso, Bindu Mangla, Experimental investigation of sustainable Corrosion Inhibitor Albumin on low-carbon steel in 1N HCl and 1N H2SO4, Results in Surfaces and Interfaces, Volume 13, 2023, 100155.

[44] Titus Chinedu Egbosiuba, Ifeanyi Emmanuel Chukwunyere, Collince Omondi Awere, Ndidiamaka Martina Amadi, Blessing Onyinye Okafor, Joseph Okechukwu Ezeugo, Okechukwu Dominic Onukwuli, Nadia Arrousse, Elyor Berdimurodov, Valentine Chikaodili Anadebe, Psidium guajava L. extract as corrosion inhibitor for mild steel in an acidic environment: Experimental and computational insights, International Journal of Electrochemical Science, Volume 20, Issue 7, 2025, 101031.

[45] Abuzar Kabir, Francesco Cacciagrano, Angela Tartaglia, Marica Lipsi, Halil Ibrahim Ulusoy, Marcello Locatelli, Chapter 7 - Analysis of monoterpenes and monoterpenoids, Editor(s): Ana Sanches Silva, Seyed Fazel Nabavi, Mina Saeedi, Seyed Mohammad Nabavi, Recent Advances in Natural Products Analysis, Elsevier, 2020, Pages 274-286, ISBN 9780128164556, doi.org/10.1016/B978-0-12-816455-6.00007-X.

[46] Ameer Jawad, Shatha K. Muallah, Kafa Khalaf Hammud, Expired Colxacillin, Amoxicillin, and Ceflaxin Drugs as Inhibitors for Low Carbon Steel Corrosion in Sodium Chloride. (2023). Al-Khwarizmi Engineering Journal, 19(1), 81-98. doi.org/10.22153/kej.2023.11.003.

[47] Dina R., Effect of Mixed Corrosion Inhibitors in Cooling Water System. (2011). Al-Khwarizmi Engineering Journal, 7(4), 76-87.

[48] Ehteram A. Noor, Temperature Effects on the Corrosion Inhibition of Mild Steel in Acidic Solutions by Aqueous Extract of Fenugreek Leaves, International Journal of Electrochemical Science, Volume 2, Issue 12, 2007, Pages 996-1017, doi.org/10.1016/S1452-3981(23)17129-X.

[49] Hussein S. Hassan, Khalid H. Rashid, Khalida F. AL-Azawi, Anees A. Khadom, Hameed B. Mahood , "Synthesis and Diagnosis of New Heterocyclic Compound as Corrosion Inhibitor for Mild Steel in Acidic Solution", DJES, vol. 17, no. 4, pp. 180–196, Dec. 2024, doi: 10.24237/djes.2024.17411.

[50] Priya Vashishth, Himanshi Bairagi, Rajni Narang, Sudhish K. Shukla, Lukman O. Olasunkanmi, Eno E. Ebenso, Bindu Mangla, Experimental investigation of sustainable Corrosion Inhibitor Albumin on low-carbon steel in 1N HCl and 1N H_2SO_4, Results in Surfaces and Interfaces, Volume 13, 2023, 100155, doi.org/10.1016/j.rsurfi.2023.100155.

[51] Mohammad Mobin, Megha Basik, Jeenat Aslam, Boswellia serrata gum as highly efficient and sustainable corrosion inhibitor for low carbon steel in 1 M HCl

solution: Experimental and DFT studies, Journal of Molecular Liquids, Volume 263, 2018, Pages 174-186.

[52] Khalid H. Rashid, Anees A. Khadom, Lei Guo,The inhibition effect of 1, 3-diazole glyoxaline on corrosion of API 5L X52 pipeline steel in oilfield produced water under sweet corrosive conditions, Results in Chemistry, Volume 7, 2024, 101528, doi.org/10.1016/j. rechem.2024.101528.

[53] Muthukrishnan, P., Prakash, P., Jeyaprabha, B. & Shankar, K. Stigmasterol extracted from Ficus hispida leaves as a green inhibitor for the mild steel corrosion in 1 M HCl solution. Arab. J. Chem. 12 (8), 3345–3356 (2019).

[54] Hameed, W.F., Rashid, K.H. & Khadom, A.A. Investigation of Tetraazaadamantane as Corrosion Inhibitor for Mild Steel in Oilfield Produced Water Under Sweet Corrosive Environment. *J Bio Tribo* Corros 8, 27 (2022).

[55] Namrata Chaubey, Vinod Kumar Singh, M.A. Quraishi, Papaya peel extract as potential corrosion inhibitor for Aluminium alloy in 1M HCl: Electrochemical and quantum chemical study, Ain Shams Engineering Journal, Volume 9, Issue 4, 2018, Pages 1131-1140.